MODELLING OF PHOSPHORUS FIRES WITH HYDROLYSIS IN THE PLUME

H.W.M. Witlox (DNV Technica, London, UK)*
John L. Woodward (DNV Technica, Temecula, USA)
M.E. Rowley and K. Sharvanandhan (Albright and Wilson, Oldbury, UK)

ABSTRACT

This paper describes the modelling of a phosphorus pool fire and the subsequent dispersion of the combustion product (phosphorus pentoxide) with hydrolysis in the plume. The commonly adopted model for hydrocarbon pool fires is generalised to allow for a phosphorus pool fire and to calculate the excess air entrainment into the fire. Transition is made from the pool-fire model to the dispersion model at 90% excess-air entrainment. The dispersion model allows the phosphorus pentoxide to react with the moisture from the air to form phosphoric acid. The sensitivity of the predictions to the location of the transition plane, the reaction rate, the relative humidity and the wind speed is investigated.

1. INTRODUCTION

A leak of liquid phosphorus from a rail car or a road tanker will result in a phosphorus fire. The worst case may be considered to be a catastrophic failure resulting in a pool fire (with a possible bund). The pool is assumed to consist of 100% liquid white phosphorus (P_4), which completely reacts with the oxygen in the air to form phosphorus pentoxide (P_4O_{10}).

Downwind of the pool fire, a cloud of solid phosphorus pentoxide disperses into the air and reacts with the moisture from the air to form liquid phosphoric acid (H_3PO_4). Formation of other acids and/or oxides is ignored. The above reaction is assumed to occur after the temperatures have reduced to moderate values.

2. POOL-FIRE MODELLING

Recent reviews of fire hazard calculations for (hydrocarbon) pool fires are given by Mudan and Croce[1], Rew et al.[2], Chapter 7 of the SINTEF handbook on fire calculations[3] and Chapter 6 of the TNO yellow book[4]. This section describes the generalisation of the original PHAST/SAFETI model[5,6] to non-hydrocarbon fires, the calculation of excess-air entrainment into the fire and subsequent smoke dispersion.

2.1 Burn rate

A cylindrical shape of the pool fire is presumed (Figure 1a). The maximum burn rate m_{max} (kg/m^2/s) on land is set by multiplying the burn velocity y_{max} (m/s) by the liquid fuel density ρ_L (kg/m^3) leading to[1]

$$m_{max} = 1.27 * 10^{-6} \rho_L \frac{\Delta H_c}{\Delta H_v^*} \quad \text{, general (incl. } P_4\text{)} \qquad (1a)$$

* Palace House, 3 Cathedral Street, London SE1 9DE, UK

$$m_{max} = 10^{-3} \frac{\Delta H_c}{\Delta H_v^*} \quad \text{, hydrocarbons} \qquad (1b)$$

where ΔH_c is the net heat of combustion (J/kg) at the boiling temperature T_b (K), $\Delta H_v^* = \Delta H_v + C_{pL}(T_b) \max\{0, T_b - T_a\}$ the modified heat of vaporisation (J/kg), ΔH_v the heat of vaporisation, C_{pL} the specific heat of the liquid, and T_a the ambient temperature. For a pool on water, the above expressions are multiplied by a factor 2.5.

The burn rate m asymptotes to its maximum value m_{max} for large values of the pool-fire diameter D,

$$m = m_{max} \left[1 - e^{-\frac{D}{L_b}} \right] \qquad (2)$$

where L_b is the characteristic length for increase of burn rate m with D. If L_b is not known, the worst-case value $m = m_{max}$ is used.

2.2 Pool-fire geometry

In case of an 'early pool fire' immediate ignition is assumed and the steady-state fire diameter D is calculated by assuming the total burn rate $[\pi D^2/4]m_{max}$ to be equal to the spill rate M (kg/s), with the upper bound of diameter being the bund diameter D_{bund} (m). In case of a 'late pool fire', liquid-pool spreading is assumed to take place prior to ignition, and the formula for the fire diameter is modified.

The widely adopted Thomas[7] correlation $H=42D\{m/[\rho_a(gD)^{1/2}]\}^{0.61}$ is used to set the flame height H in terms of the flame diameter D, the burn rate m and the ambient density ρ_a. The tilt angle φ is set using an AGA formula[8].

2.3 Radiation

The surface emissive power of the flame is defined by

$$E_f = E_m \left[e^{-\frac{D}{L_s}} \right] , \quad \text{luminous fires} \qquad (3a)$$

$$= E_m \left[e^{-\frac{D}{L_s}} \right] + E_s \left[1 - e^{-\frac{D}{L_s}} \right] \quad \text{sooty fires} \qquad (3b)$$

$$= \chi_R \, m \, \Delta H_c / [1 + 4(H/D)] \quad \text{'general' fire (incl.P}_4\text{)} \qquad (3c)$$

where E_m is the maximum emissive power for luminous fires, E_s the smoke emissive power[1], and L_s a characteric length for decay of E_f. If experimental values for E_m, E_s, L_s are not available, Equation (3c) is used[4]. Here the radiative fraction χ_R is defined to be the ratio of total energy radiated (from the fire surface) to the total energy released (from pool area). The radiation intensity received by a given plane through a given point can be derived by multiplying E_f by the view factor F (including the effects of atmospheric absorption)[5].

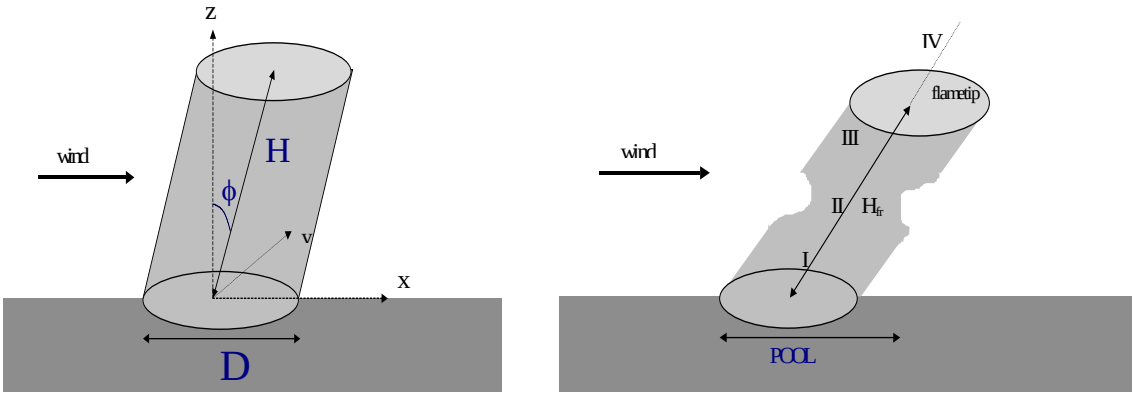

Figure 1. Pool-fire model; (a) geometry (diameter D, height H, tilt angle ϕ), (b) entrainment zones (I. near pool fire, II. neck-in area, III. below flame tip, IV. above flame tip)

2.4 Excess-air entrainment

The pool-fire excess-air entrainment is taken from correlations by Delichatsios[9] based on experimental data and similarity arguments. The excess air entrainment M_{entr} (kg/s) is set as a function of the ratio Z/D, where Z is the axial height along the flame cylinder and D the flame diameter. This function is expressed in terms of the Froude number Fr and the 'Froude' flame height H_{fr} defined to be the height at 90% excess-air entrainment. He distinguishes between the following zones (Figure 1b): zone I - close to the pool fire [$Z < \min(D,H_{fr})$], zone II - in or beyond the neck-in area [$\min(D,H_{fr}) < Z < \min(5D,H_{fr})$], zone III - above the neck-in area and below the flame tip [$\min(5D,H_{fr}) < Z < H_{fr}$], and zone IV - above the flame tip [$Z > H_{fr}$],

$$Fr\frac{M_{entr}}{(1+\chi_a S_{thw})M} = 0.086\,(Z/D)^{0.5}, \quad \text{zone I}$$

$$= 0.093\,(Z/D)^{1.5}, \quad \text{zone II}$$

$$= 0.018\,(Z/D)^{2.5}, \quad \text{zone III}$$

$$= 0.21Fr^{1/3}\,[(Z-H_{fr}+10.21Fr^{0.4})/D]^{5/3}, \quad \text{zone IV}$$

where χ_a is the combustion efficiency, S_{thw} the stoichiometric mass ratio of wet air to fuel, and M the mass flow (kg/s) of the initial liquid fuel. See the paper by Delichatsios for expressions for the Froude number Fr, and the Froude flame height H_{fr}.

The pool is assumed to consist of 100% liquid white phosphorus (P_4), which completely reacts with the oxygen in the air to form phosphorus pentoxide (P_4O_{10}). The reaction is: $P_4 + 5O_2 \rightarrow P_4O_{10}$. The theoretical stoichiometric mass ratios S_{th} = 5.54 is defined to be the mass ratio of dry air to fuel (P_4) needed in case of complete combustion. The mixture composition is now derived from the above formula, the composition of the moist air (water, oxygen, nitrogen; mass fraction of oxygen in dry air is 0.233), and the values of S_{th} and S_{thw}:

- mass flow of combustion product (pollutant) = $M_{pol} = (1+\chi_A S_{thw})\,M$:
  - mass flow of unburned fuel $M_{unb} = (1-\chi_A)M$
  - mass flow of combustion oxide $M_{oxi} = \chi_A\,(1 + 0.233S_{th})\,M$
  - mass flow of initial nitrogen $M_{N2} = \chi_A\,(0.767S_{th})\,M$
  - mass flow of initial water $M_{H20} = \chi_A\,(S_{thw}-S_{th})\,M$
- mass flow of excess air entrainment = M_{entr}

- total mass flow (kg/s) of the mixture $M_{tot} = M_{entr} + M_{pol}$

where χ_A is the combustion efficiency (complete combustion χ_A=1 is assumed here).

2.5 Plume temperature

The final mixture temperature can be obtained by equating the final enthalpy to the initial enthalpy (prior to the mixing). The following simplifying assumptions are being made:

- the initial fuel is liquid, with a liquid-pool temperature of T_p ($T_p<T_b$)
- all water is assumed to be in the vapour phase; this assumption is justifiable given the high fire temperatures likely to arise
- the specific heat of dry air is constant and equals 1004 J/kg/K
- the specific heats of nitrogen and water-vapour are constant, and equal 1130, 2160 J/kg/K respectively (values at approx. 550K); this may lead to less accurate results for very high temperatures, but is likely to be reasonably accurate at the point of transition with the dispersion model, i.e. at 90% excess air entrainment
- the specific heat of the combustion oxide is constant, and its value is taken to be at the fuel boiling temperature T_b
- the combustion oxide is assumed to be solid (solid smoke particles)
- combustion occurs immediately after evaporation; no further combustion occurs
- the unburned fuel is assumed to be liquid

The mixture density is obtained from the ideal-gas law while ignoring the volumes of solids and liquids.

3. DISPERSION MODELLING

The transition from the pool-fire model to the dispersion model is illustrated in Figure 2. It is presumed to take place at the Froude flame height H_{fr} previously defined (at 90% excess air entrainment), in a plane with tilt angle ϕ. The following data at the transition plane are provided by the pool-fire model:

- mixture composition: flows of fuel, stoichiometric air and excess air (kg/s)
- plume velocity (m/s)
- plume temperature (K)
- transition plane: vertical height (m) and plume angle (degrees)

The Unified Dispersion Model UDM[10,5] treats a positively or negatively buoyant plume accounting for temperature change with entrained air and momentum exchange with the wind. It predicts plume rise, bending angles, plume touchdown, particle trajectories, rain out, re-evaporation from a pool, and initial dilution across a pool.

The UDM is a similarity model in which the form of concentration and velocity profiles are assumed. The cross-wind and the vertical directions can start as sharp-edged profiles which become more diffuse further away from the source. The cross-sectional area is an ellipse while aloft, and becomes a hemi-ellipse upon touchdown.

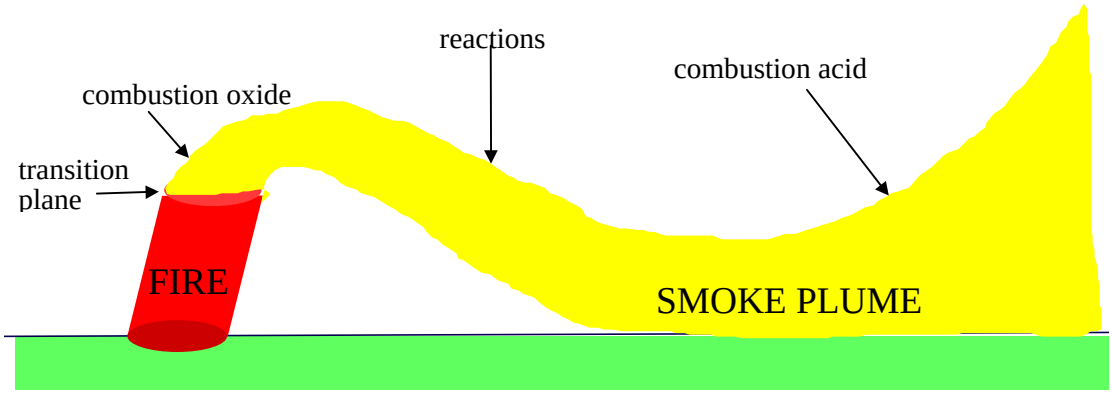

Figure 2. Transition from pool-fire model to dispersion model UDM

Particle and droplet trajectories are calculated by integrating ordinary differential equations containing buoyancy and drag terms as well as evaporation and condensation. Evaporation is calculated using a non-equilibrium model which accounts for heat and mass transfer rates to the droplets. A mono-disperse drop size distribution is assumed, which gives rise to a single point of rain out. When the drops touches down all of the remaining mass of liquid or solid in the plume is modelled as raining out.

The UDM model is extended as part of the present project to allow for the transition from the pool-fire model. In the case of phosphorus, it includes the reaction of phosphorus pentoxide with water to form phosphoric acid (P_4O_{10}+6 H_2O = 4 H_3PO_4). The thermodynamics has also been extended to allow for the presence of solid particles (i.e. solid phosphorus pentoxide and phosphoric acid). A zero-order reaction rate equation $\partial w_{R2}/\partial t = -k$ is assumed. Here t is the time, w_{R2} the mass fraction of reactant 2 (water), and k the reaction rate. Note that k is assumed to be constant [no temperature dependency] Furthermore rainout is only modelled for phosphorus pentoxide (reactant 1).

4. RESULTS

4.1 Base-case problem

The above pool-fire and dispersion models have been implemented as new models (called PFGEN and UDM) in a new test version of PHAST. First results are presented for a base-case problem chosen to correspond to conditions typical for a (worst-case) accidental release of phosphorus.The properties are as chosen as follows:

- phosphorus properties: m = m_{max} assumed, ΔH_c = 2.47E7 J/kg, χ_A = 1, χ_R = 0.35, k = 0.5, heat of hydrolysis reaction = 1.51E6 J/kg of P_4O_{10}, other properties from DIPPR database
- pool data: bund length = 15 m, bund width = 5 m, liquid temperature = 70^{o}C, elevation = 0 m
- ambient data: wind speed = 5 m/s, pressure = 1 atm., temperature = 10^{o}C, relative humidity = 70%
- dispersion data: surface roughness = 0.17 m

The catastrophic failure is assumed to lead to such a large liquid spill rate ($\geq$ 5.64 kg/s) that a steady-state pool-diameter can be assumed equal to the bund diameter.

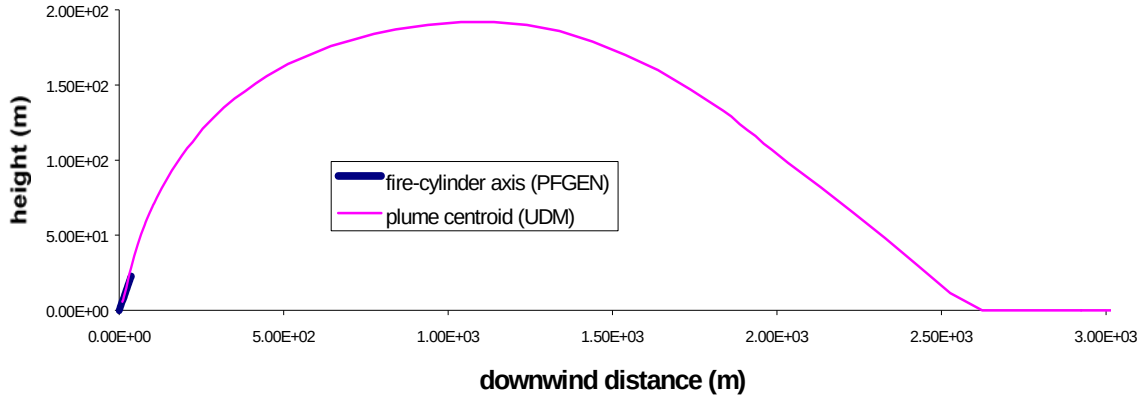

Figure 3. PFGEN/UDM predictions of movement of plume centroid

Figure 3 displays the position of the fire-axis/plume centroid leaving the fire and propagating downwind. At the point of transition, the UDM predictions of the plume centroid are indeed tangent to the fire axis. Due to high-temperature buoyancy effects, the plume first rises. Then the plume becomes heavier than air by cooling leading to plume subsidence.

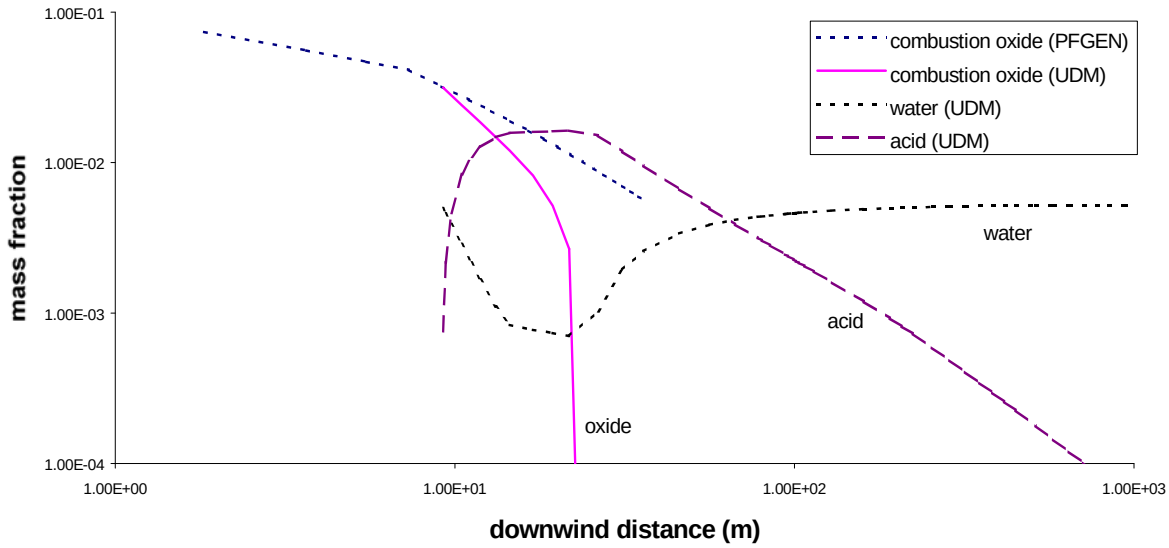

Figure 4. PFGEN/UDM predictions of mass fractions in flame/plume

Figure 4 displays the combined PFGEN/UDM predictions of the concentrations of the combustion oxide, acid and water without time averaging. No reaction of water is presumed in the hot pool-fire regime. Following the pool-fire transition it is seen that the combustion-oxide rapidly disappears due to reaction with water. Consequently water decreases as long as oxide is present and then levels out at ambient density. The acid concentration is at its peak at the point of disappearance of the combustion oxide. Downwind of this point the acid concentration reduces due to air entrainment into the cloud mixture.

4.2 Sensitivity analysis

A sensitivity analysis is carried out to study the effect of parameter variations to the base-case problem. Figures 5-8 include results for the variation of the transition point, rate of reaction, relative humidity, and wind speed.

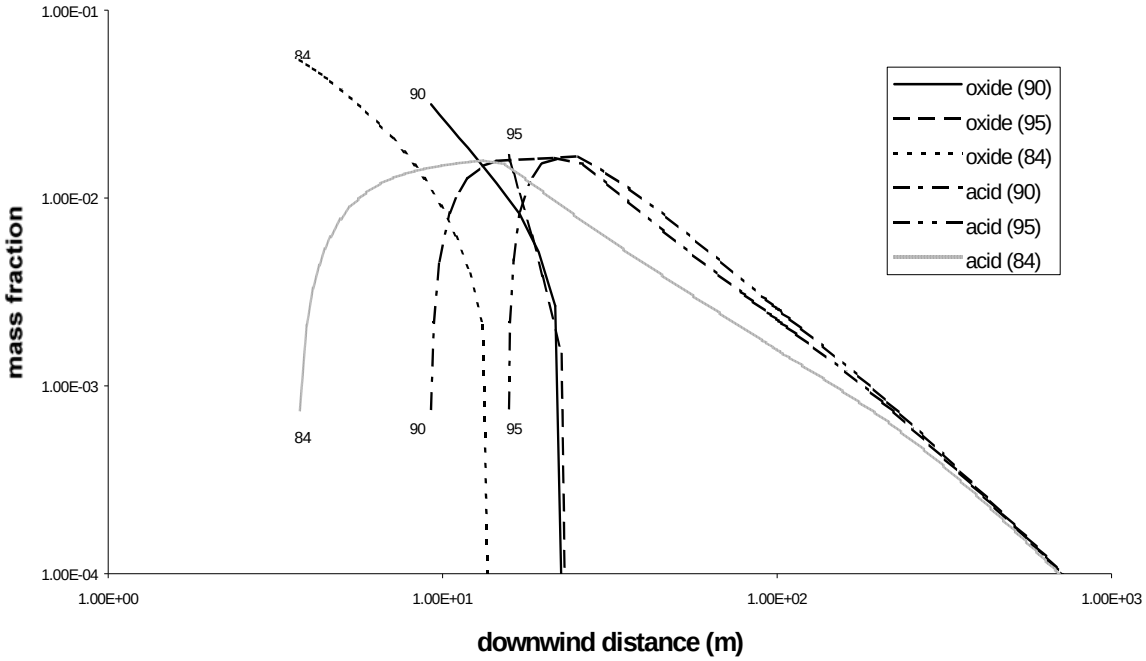

Figure 5. Effect of transition point on predictions of mass fractions of P_4O_{10}, H_3PO_4 (transition point at 90, 95, 84 % excess air)

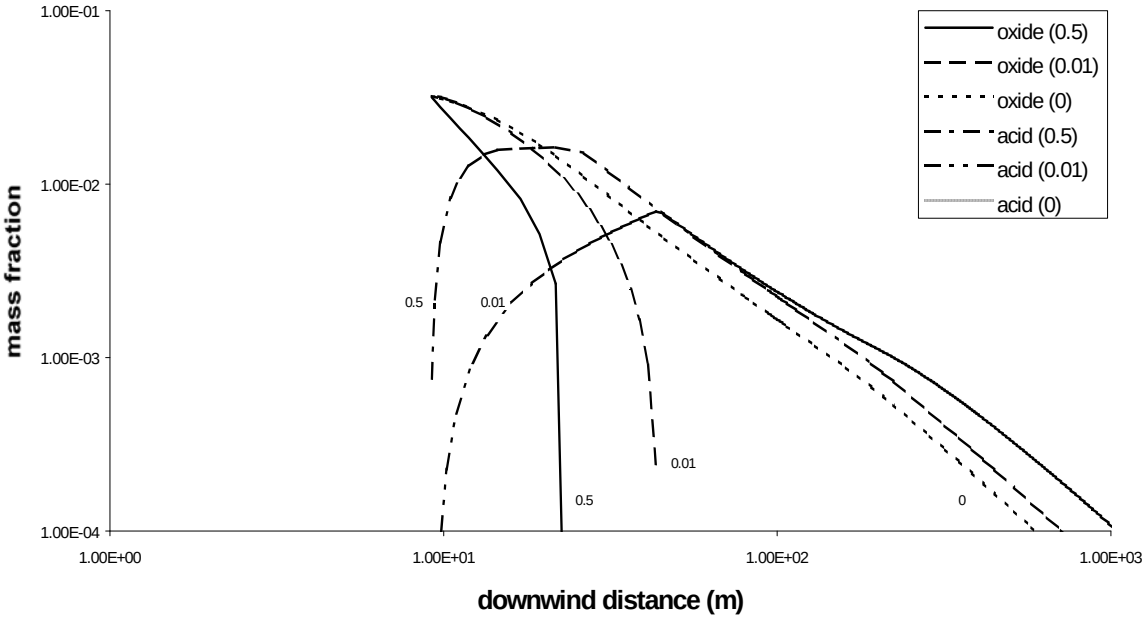

Figure 6. Effect of reaction rate on predictions of mass fractions of P_4O_{10} and H_3PO_4 (reaction rate constant = 0.5, 0.01, 0)

In Figure 5 two additional runs are carried out with respectively an early PFGEN/UDM transition point (84 % excess-air entrainment) and a late transition point (at the Thomas axial flame height and 95 % excess-air entrainment). At a later transition point, the P_4O_{10} more readily disappears because of the larger amount of water available from the excess moist air. As expected, further downwind the difference in mass fractions diminishes for the different transition points.

In Figure 6 the effect of the reaction-rate is studied: k = 0.5 (base-case value), 0.01 (small reaction rate), 0.00 (no acid formation). It is indeed observed that the P_4O_{10} concentrations are larger for smaller reaction rates.

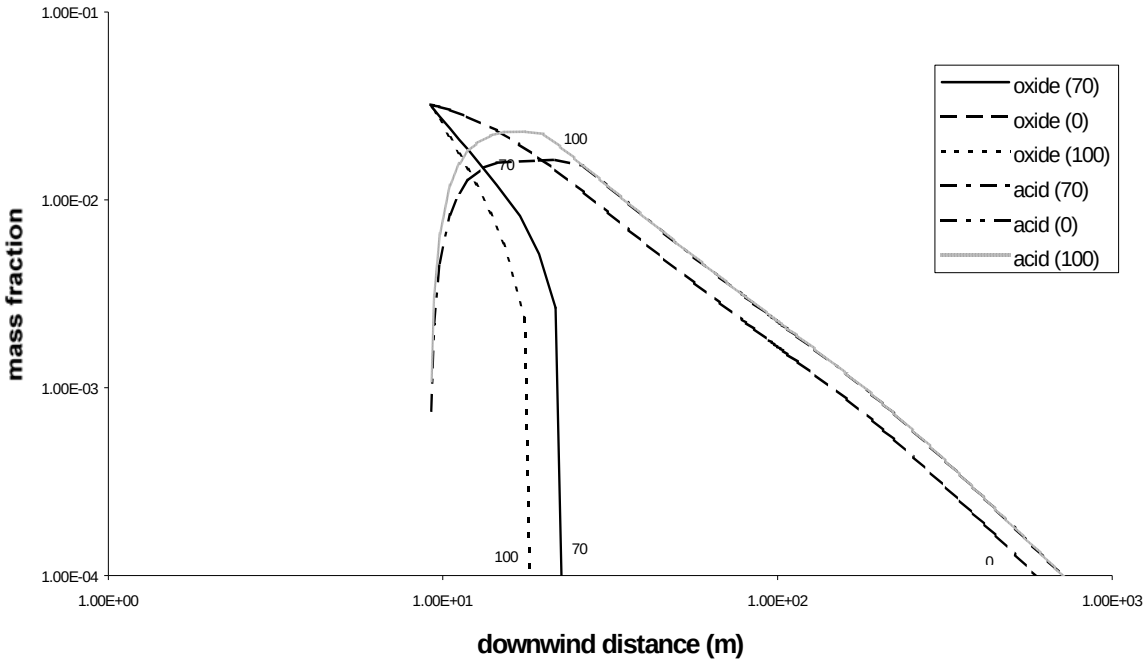

Figure 7. Effect of relative humidity on predictions of mass fractions of P_4O_{10}, H_3PO_4 (relative humidity = 0,70,100 %)

In Figure 7 the effect of the variation of relative humidity is studied: r_H = 0% (no water), 70% (base case), 100%. Naturally no acid forms in the absence of water, and acid formation (P_4O_{10} disappearance) is quicker with increasing humidity.

Figure 8 shows results with a variation of the wind speed u_o at stability class D: 2 (low value), 5 (base-case), 15 m/s (extreme large value). Note that for very large wind speeds the 'fire cylinder' will actually 'hit' the ground (distance between the fire axis and ground is less than the fire diameter!) and the validity of the results may be more dubious. This applies both for the radiation results (i.e. based on zero wind-speed Thomas flame length) and the pool-fire excess-air formulation of Delichatsios (i.e. based on zero wind-speed experiments). Following the transition, the UDM model therefore immediately 'touches down' for large wind speeds.

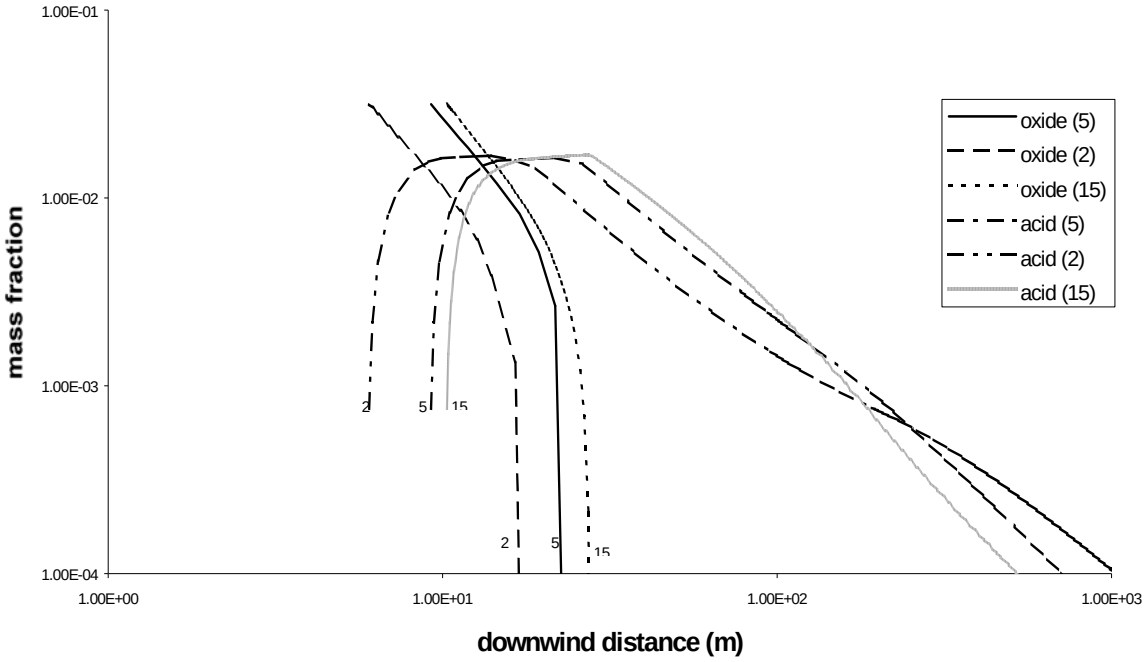

Figure 8. Effect of wind speed on predictions of mass fractions of P_4O_{10}, H_3PO_4 (wind speed at 5, 2, 15 m/s)

5. FURTHER DEVELOPMENTS

1. More accurate modelling of non-zero wind-speed effects may involve:
   - An alternative more appropriate flame-length formula[11].
   - The excess-air entrainment formulation by Delichatsios[9] is based on zero wind-speed experimental data, and needs extension for non-zero wind speeds.
   - An elliptical cross section (larger diameter in the downwind direction) for the fire rather than a circular one will be more accurate (wind-speed drag)[2].
2. The model has so far been applied to modelling of phosphorus only, and may be further extended to other types of fires. In case of hydrocarbons, this will involve taking into account the generation of water as part of the combustion reaction. This will have an effect on the calculations of the mixture composition and the pool-fire thermodynamics. Also the excess-air entrainment formulation may need further extension for small stoichiometric air to fuel ratios (near to 1).
4. More accurate description of the pool-fire thermodynamics, and incomplete combustion (e.g. presence of both carbon monoxide and carbon dioxide).
5. Further validation against experimental data is desirable (air entrainment, fire dimensions, radiation, smoke generation).
6. The model now provides a transition from a pool-fire model to smoke dispersion. An additional model may be developed for a link between a turbulent jet flame and smoke dispersion. Herewith use may be made of the formulation of Delichatsios for small Froude numbers.

7. More accurate kinetic rate constants are needed. The reaction rate constant has been varied only in order to compare the difference between zero, slow, fast and complete reaction. Further improvements could include formation of other phosphoric acids and phosphorus oxides, temperature-dependency of reaction rate, reactions for other compounds (ammonium, sulphide trioxide, phosphine, phosphorus chlorides,....), incomplete reactions (equilibrium constants), and multi-compound rainout (i.e. both reactants and products)

6. REFERENCES

[1] Mudan, K.S., "Fire hazard calculations for large open hydrocarbon fires", Section 3-11 in "SFPE handbook of fire protection engineering", Second Edition, National Fire Protection Association, Quincy, MA (1995)

[2] Rew, P.J., Hulbert, W.G., and Deaves, D.M., "Modelling of thermal radiation from external hydrocarbon pool fires", Trans. IchemE 75, Part B, pp. 81-89 (1997)

[3] "Handbook on fire calculations and fire risk assessment in the process industry", SINTEF, Norway (1992)

[4] Engelhard, W.F.J.M., "Heat flux from fires", Ch. 6 in "Methods for the calculation of physical effects", CPR14E, Part 2 (TNO Yellow Book), SDU Uitgevers, The Hague (1997)

[5] DNV Technica, "SAFETI software for the assessment of flammable explosive and toxic impact - Theory Manual", Version 3.4, DNV, London (1996)

[6] Cook, J., Bahrami, Z., and Whitehouse, R.J., "A comprehensive program for calculation of flame radiation levels", Proceeding of First Int. Conf. on Loss of Containment, London, UK (1989)

[7] Thomas, P.H., "The size of flames from natural fires", 9th Int. Combustion Symposium, Comb. Inst., Pittsburgh, PA, pp. 884-859 (1963)

[8] "LNG safety research program", Report IS-3-1, American Gas Association (1974)

[9] Delichatsios, M.A., "Air entrainment into buoyant jet flames and pool fires", Section 3-2 in "SFPE handbook of fire protection engineering", Second Edition, National Fire Protection Association, Quincy, MA (1995)

[10] Woodward, J.L, Cook, J., and Papadourakis, A., "Modelling and validation of a dispersing aerosol jet", Journal of hazardous materials 44, pp. 185-207 (1995)

[11] McCaffrey, "Flame Height", Section 1-2 in "SFPE handbook of fire protection engineering", Second Edition, National Fire Protection Association, Quincy, MA (1995)